Influence of cyclic-loading induced fatigue micro-crack growth on generation of nonlinear ultrasonic Lamb waves

Taotao Ding[1] · Wujun Zhu[1] · Congyun Ma[1] · Yanxun Xiang[1] · Mingxi Deng[2] · Fu-zhen Xuan[1]

Abstract

Fatigue damage and micro-cracks growth have been proved to be closely related to the nonlinear effect of ultrasonic Lamb waves propagation in materials. In this paper, the relationship among fatigue life, length and width of micro-cracks, and the acoustic nonlinearity parameter was established. The variation of the acoustic nonlinearity parameter caused by fatigue damage was analyzed based on micro-cracks growth. Considering the multimodal nature of nonlinear Lamb waves, we selected the low-frequency mode pairs S0–s0 and S1–s2 to evaluate fatigue damage in 7075 aluminum alloy plates. Both FE simulations and experiments show that the mode pair S1–s2 is more suitable than S0–s0 for the assessment of fatigue damage. It was found that with increasing fatigue cycles, the relative acoustic nonlinearity parameter A_2/A_1^2 firstly increases because the micro-cracks length extends while the micro-cracks width does not change much. The relative acoustic nonlinearity parameter A_2/A_1^2 reaches its peak at about 60% of the fatigue life. Then the relative acoustic nonlinearity parameter A_2/A_1^2 decreases because of the rapid increase in the micro-cracks width. Our findings clarify the mountain-shape curve between the relative acoustic nonlinearity parameter A_2/A_1^2 and the fatigue cycles.

Keywords Nonlinear Lamb waves · Fatigue damage · Third-order elastic constants · Micro-cracks

1 Introduction

Plate structures like oil tanks, pressure vessels, wind turbine blades, aircrafts, etc. operate often under severe conditions for long period of time. In practical applications of these plate-like structures, the material degradation, such as fatigue damage, creep damage, and plastic deformation, etc., is caused by internal factors and external environment. In the incipient stage of material degradation, the dislocation density increases significantly and vacancy clusters are generated. After that, growth, aggregation and formation of micro-cracks are observed. In the last stage, macro-cracks

are formed until fracture of the material. Several studies have shown that the incipient stage of material degradation occupy most of their life for well-designed components [1]. For example, under cyclic loading, the incipient stage of material degradation takes about 80–90% of the fatigue life [2, 3]. At high temperature and low stress, the incipient stage of material degradation assumes about more than 70% of the creep life [4]. Therefore, effective detection and characterization of incipient damage of materials is of great significance for the life prediction of components.

Fatigue damage will change the microstructure of materials. The second-order elastic constant changes slightly, but the third-order elastic constants change significantly [5, 6]. The second-order elastic constant reflects the linear behavior of material and determines the propagation velocity and attenuation of ultrasonic waves in the material. Since the variation of sound velocity with stress, waveform distortion and high harmonic excitation caused by nonlinear behavior leads to change of third-order elastic constants, the incipient stage of material degradation can be characterized by monitoring third-order elastic constants. A growing number of studies have shown that the degradation of material properties is related to the nonlinear effect of ultrasound [7–12]. It

✉ Wujun Zhu
wujunzhu@ecust.edu.cn

✉ Yanxun Xiang
yxxiang@ecust.edu.cn

1   Key Laboratory of Pressure Systems and Safety, MOE.
    School of Mechanical and Power Engineering, East China
    University of Science and Technology, Shanghai 200237,
    China

2   College of Aerospace Engineering, Chongqing University,
    Chongqing 400044, China

was reported that the evolution of microstructures results in nonlinear mechanical behavior of materials [13–15]. At the incipient stage of material degradation, ultrasound exhibits obvious nonlinear effect and produces high order harmonics and sub-harmonics. The variation of acoustic nonlinearity parameter is ascribed to both the second-order and the third-order elastic constants. However, the acoustic linear parameters, such as the wave velocity and attenuation, depend on the second-order elastic constants, and the third-order elastic constants contribute mainly to the acoustic nonlinearity parameter. Thus, the damage evolution in the incipient stage of fatigue life can be essentially characterized by the increase of the third-order constants.

Most recent studies have focused on nonlinear ultrasonic Lamb waves using second harmonics to characterize quantitatively the incipient stages of damage in plate-like structures. Compared with bulk waves, Lamb waves provide more efficient volumetric coverage of a structure and can monitor regions inaccessible to bulk waves, which has attracted attention of many scholars [15–18]. As to plastic deformation and fatigue damage, the research mainly focuses on the relationship between acoustic nonlinearity parameter and the fatigue life of materials. According to literature, the relationship between acoustic nonlinearity parameter and fatigue life can be divided into three forms, namely, non-linear monotonous rise, monotonous fall and non-monotonous. For example, Jhang [19] observed that the acoustic nonlinearity parameter of steel SS41 and SS45 increases with the fatigue cycle. Kim et al. [20] measured the acoustic nonlinearity parameter of polycrystalline pure copper and copper alloy Cu-35Zn with the same strain amplitude. The results show that the acoustic nonlinearity parameter increases monotonously with the increase of fatigue damage. However, Deng [21] used nonlinear ultrasonic Lamb waves to detect the fatigue damage of aluminum plates. A parameter, $SWF_r(2f)$, was termed the stress wave factor of second harmonics generated by primary Lamb waves, which decreases monotonously with the increase of fatigue cycles. In addition, Sagar et al. [22] measured the low-cycle fatigue damage of pearlite steels using nonlinear longitudinal waves, and the acoustic nonlinearity parameter shows a mountain shape curve with the fatigue damage. Similar results have been found in other studies [23–25]. All these studies show the relationship between acoustic nonlinearity parameter and fatigue damage, but the mechanism behind has not yet been fully understood.

With the accumulation of fatigue damage, micro-cracks gradually form and grow in the plate. When the macro-cracks length reaches a certain threshold, the material will fracture in a short time. In general, the micro-cracks are too small to detect with traditional ultrasonic testing at the incipient stages of fatigue [20]. Deng and Pei [21] used nonlinear ultrasonic Lamb waves to detect fatigue damage of

an aluminum plate, and pointed out that the formation and growth of micro-cracks increase the attenuation of acoustic waves propagating in the plate and reduce the efficiency of second harmonic generation. Jiao et al. [26] studied the nonlinear interaction between micro-crack and Lamb waves using the finite element method, and successfully detected surface fatigue cracks. Wan et al. [27] obtained the relationship between A_2/A_1^2 and micro-cracks length and width through simulation. Shen et al. [28, 29] used a highly efficient numerical model to analyse the nonlinear features of scattered waves from fatigue cracks, taking into consideration the rough surface condition of the cracks. Hafezi et al. [30] developed the peri-ultrasound model to detect the waves generated by the applied load and the crack propagation resulted from the shear load. The previous studies mainly focused on the relationship between acoustic nonlinearity parameter and fatigue damage in the incipient stage of fatigue life. The generation mechanism of second harmonic Lamb waves in the whole fatigue life of structures, from the fatigue damage accumulation to micro-crack initiation and propagation, has not yet been fully investigated.

In this paper, third-order elastic constants were changed to simulate the fatigue damage of an Al7075 aluminum alloy by FE simulations. The excitation efficiency of nonlinear ultrasonic Lamb wave mode pairs S0–s0 and S1–s2 and their sensitivity to the third-order constants were studied. In addition, the variation of the relative acoustic nonlinearity parameter A_2/A_1^2 was analyzed by observing the length and width of the micro-cracks by means of an optical microscope. The length and width of the micro-cracks at the inflexion point of acoustic nonlinearity parameter were determined.

2 Theoretical Consideration

In the process of propagation in a material, ultrasonic waves are distorted, and consequently high-order harmonics are generated. The microstructure-related elastic constants of the material can be represented by the amplitude of high-order harmonic generation. There is a certain correlation between the elastic constants and acoustic nonlinearity parameter.

For solid material applied with fatigue load, the nonlinear constitutive relation is

$$\sigma_{ij} = \sigma_{ij}^0 + A_{ijkl}\frac{\partial u_k}{\partial X_l} + \frac{1}{2}A_{ijklmn}\frac{\partial u_k}{\partial X_l}\frac{\partial u_m}{\partial X_n} + ..., \quad (1)$$

where, σ_{ij}^0 is the initial stress of the material, σ_{ij} is the stress tensor, u_k is the wave displacement of the particle, A_{ijkl} and A_{ijklmn} are the second-order and third-order Huang coefficients, respectively [31].

The propagation of one-dimensional ultrasonic longitudinal waves in isotropic materials is solved. By substituting Eq. (1) into the wave equation of ultrasonic waves propagation in solid materials, the nonlinear waves equation is obtained as follows

$$\frac{\partial^2 u_1}{\partial t^2} = c^2 \frac{\partial^2 u_1}{\partial X_1^2}\left[1 - \beta \frac{\partial u_1}{\partial X_1}\right], \tag{2}$$

where $c = \sqrt{\left(\overline{C}_{1111} + \sigma_{11}^0\right)/\rho}$ is the propagation velocity of the longitudinal waves, β is the acoustic nonlinearity parameter given by

$$\beta = -\frac{\overline{C}_{111111} + 3\overline{C}_{1111}}{\overline{C}_{1111} + \sigma_{11}^0}, \tag{3}$$

where $\overline{C}_{1111}$ and $\overline{C}_{111111}$ are the second-order elastic constant (SOEC) and the third-order elastic constant (TOEC) of the one-dimensional model, respectively, and σ_{11}^0 is the initial stress of the material. The second-order elastic constants $\overline{C}_{1111}$ and the initial stress σ_{11}^0 change little under the fatigue load. Equation (3) indicates that the nonlinearity parameter of the material is related to the magnitude of the third-order elastic constants. In the process of fatigue damage, the evolution of microstructure changes the third-order elastic constants, which in turn changes the acoustic nonlinearity parameter. Consequently, the acoustic nonlinearity parameter can be used to monitor the change of microstructure [32].

In addition, the acoustic nonlinearity parameter can be expressed as a function of fundamental amplitude A_1 and harmonic amplitude A_2 as follows

$$\beta = -\frac{8A_2}{\kappa^2 X_1 A_1^2}, \tag{4}$$

where κ is wavenumber. Above equations describe the relationship among fatigue damage, the third-order elastic constants and the acoustic nonlinearity parameter. Here, we determine the acoustic nonlinearity parameter via FE simulations and experiments, so that we can indirectly understand the microstructure evolution of materials and the degradation of mechanical properties caused by fatigue damage.

3 Numerical Simulation Analyses

3.1 Simulation Settings and Mode Selection

FE simulation of nonlinear Lamb wave propagation in a 2-mm-thick 7075 aluminum alloy plate was performed to evaluate fatigue damage using the commercial software Abaqus/EXPLICIT. We incorporated the nonlinear constitutive relationship and the Green–Lagrange strain tensor in a subroutine VUMAT using FORTRAN, a compiled imperative programing language, for an isotropic and homogenous material in order to construct both the convective and inherent nonlinearities, regardless of the material's attenuation and dispersion. The material parameters of 7075 aluminum alloy are listed in Table 1, where ρ is the density, λ and μ are Lame constants, A, B and C are Landau-Lifshitz TOECs, $\overline{C}_{1111} = \lambda + 2\mu$, and $\overline{C}_{111111} = 2A + 6B + 2C$. A two-dimensional model was established with the length of 1000 mm and the upper and the lower surfaces were traction-free, as shown in Fig. 1. The rectangle with elements of 0.05 mm size was used for meshing the two-dimensional model, which is smaller than the spatial resolution $\lambda/20$, where λ is the wavelength. The time step was set to 1×10^{-8} s, much smaller than the time resolution $\Delta d/v_g$, where v_g is the group-velocity of the targeted Lamb mode. This setting can not only ensure the error convergence and calculation accuracy, but also meet the stability criteria. Received time-domain signals were analyzed by Short Time Fourier Transform (STFT) to obtain the amplitudes of the primary and the second harmonic Lamb waves, then the relative acoustic nonlinearity parameter was calculated by $\beta = A_2/A_1^2$.

In this section, an excitation source was set at the left end of the model, and a receiver was placed at the right of the model to pick up the in-plate displacements at the upper surface of the plate. Excitation signal was applied by imposing displacements on the left edge with
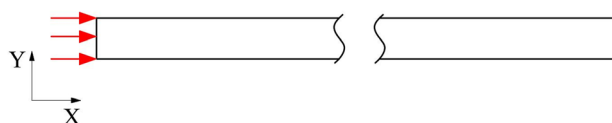
Fig. 1 Schematic diagram of a two-dimensional FE simulation model

Table 1 Material parameters of the 7075 aluminum alloy [33]

Material	Density	Lame constants		SOEC of one dimensional model	Landau-Lifshitz TOECs			SOEC of one dimensional model
	ρ (kg.m³)	λ (GP)	μ (GPa)	$\overline{C}_{1111}$ (GPa)	A (GPa)	B (GPa)	C (GPa)	$\overline{C}_{111111}$ (GPa)
Al7075	2757	57.3	27.3	111.9	− 350	− 158	− 92	− 1832

a 20-cycle Hanning-windowed sinusoidal tone burst. The dispersion curves of the 2-mm-thick Al7075 aluminum alloy plate are shown in Fig. 2, where the red and blue curves represent the symmetric and asymmetric mode of ultrasonic Lamb waves, respectively. Here, the low-frequency mode pairs S0–s0 and S1–s2 were selected for FE simulations and nonlinear ultrasonic Lamb waves experimental measurements of fatigue damage. In the low-frequency region, there are only two modes, and the dispersion nature of the mode pair S0–s0 is restrained. Hence, the measurement difficulties caused by the dispersion and multimode nature of the nonlinear ultrasonic Lamb waves can be relieved. However, this low-frequency region has a large frequency range, over which the mode pair S0–s0 shows quasi phase-velocity matching. Hence, the excitation frequency needs to be determined by considering the cumulative growth with the propagation distance. The mode pair S1–s2 shows exact phase-velocity matching at a frequency of 1.8 MHz, hence the optimal excitation frequency of the mode pair S1–s2 is 1.8 MHz.

The excitation frequency of Lamb waves mode pair S0–s0 was set to be 100 kHz, 150 kHz, 200 kHz, 250 kHz, 300 kHz, 400 kHz at the FE simulations, respectively. Figure 3 shows the relative acoustic nonlinearity parameter A_2/A_1^2 as a function of the propagation distance at different excitation frequencies. The A_2/A_1^2 oscillates along the propagation distance sinusoidally, and the oscillation period becomes shorter with increasing excitation frequency. In view of the fact that on one hand it is difficult to achieve the excitation signal at low frequency, and on the other hand the cumulative distance is short at high frequency which is not conducive to the experimental measurement, the excitation frequency of Lamb waves mode pair S0–s0 was determined to be 300 kHz.
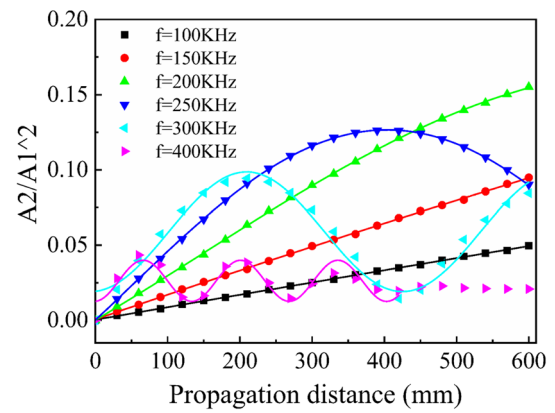

Fig. 3 Relative acoustic nonlinearity parameter A_2/A_1^2 with respect to the propagation distance for mode pair S0–s0 at various excitation frequency

3.2 Effect of Third-Order Elastic Constants

The variation of acoustic nonlinearity parameter is ascribed to both second-order constants and third-order constants, while the linear ultrasonic is only dependent on second-order constants. Since acoustic nonlinearity parameter grows dramatically, and the linear acoustic parameter changes slightly at the incipient stage of fatigue damage, it is reported that third-order constants mainly contributes to the variation of acoustic nonlinearity parameter [34]. Third-order elastic constants A, B and C are assumed to increase by 0, 10% and 30% in this work. Figures 4a and 5a show the normalized relative acoustic nonlinearity parameter A_2/A_1^2 as a function of the propagation distance when the third-order elastic constants were increased by 0, 10% and 30%, respectively. The slope of the normalized A_2/A_1^2 with the propagation distance was obtained by linear fitting, and it increases obviously with increasing third-order elastic constants of the material.
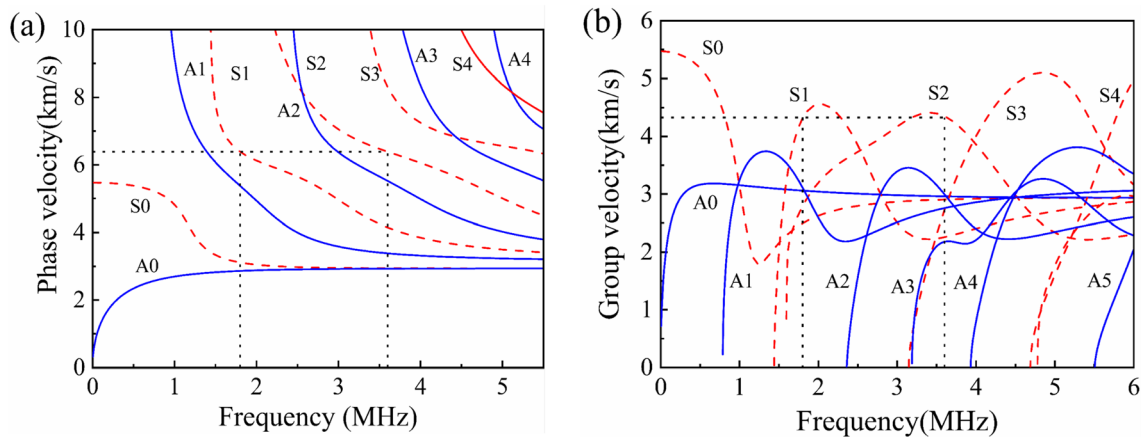

Fig. 2 The phase velocity dispersion curves (**a**) and group velocity dispersion curves (**b**) of a 2- mm-thick Al7075 plate
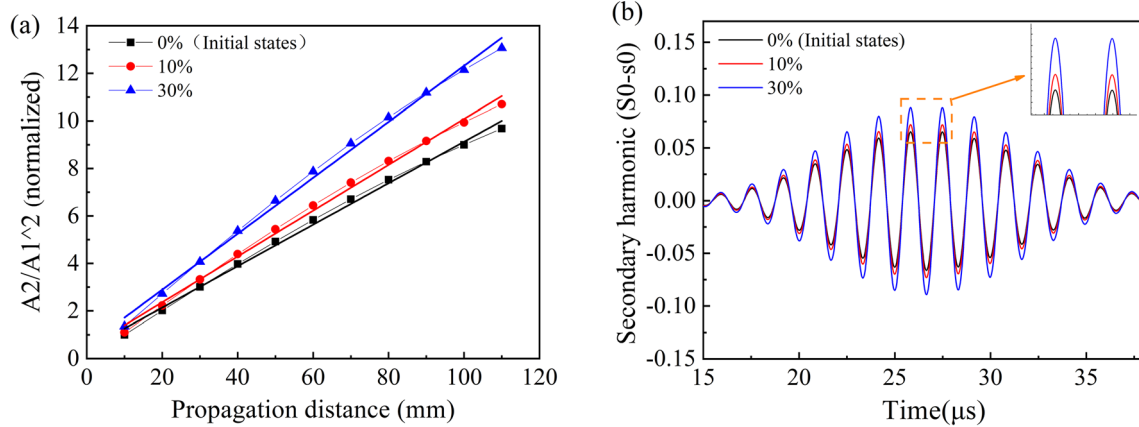
Fig. 4 **a** Relative acoustic nonlinearity parameter A_2/A_1^2 as a function of the propagation distance and **b** the harmonic signals at a propagation distance of 100 mm for mode pair S0–s0 with the third-order elastic constants increased by 0, 10% and 30%, respectively
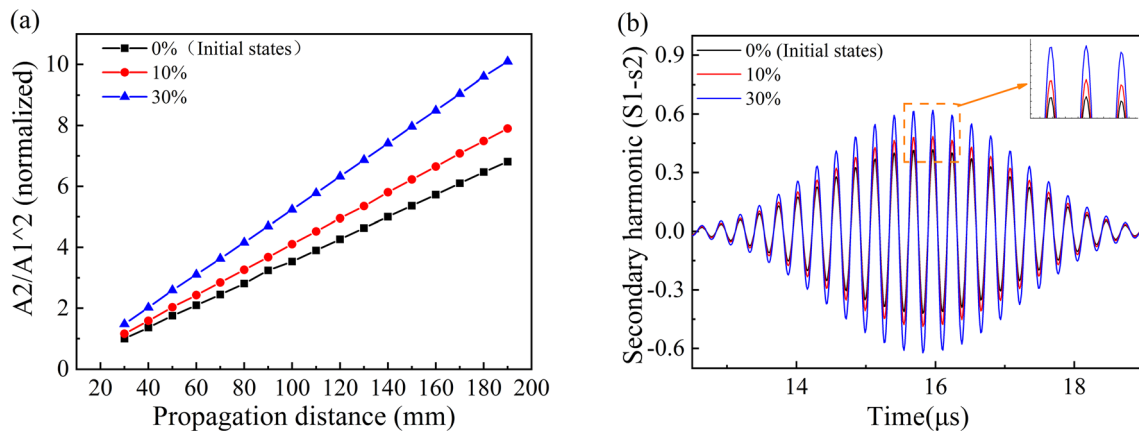

Fig. 5 **a** Relative acoustic nonlinearity parameter A_2/A_1^2 as a function of the propagation distance and **b** the harmonic signals at a propagation distance of 60 mm for mode pair S1–s2 with the third-order elastic constants increased by 0, 10% and 30%, respectively

Figures 4b and 5b show the filtered time-domain second harmonic signals with different third-order elastic constants. Time-domain signals received at pre-designed propagation distances were filtered, and the filtering range was 500 -700 kHz and 3–4.2 MHz for mode pairs S0–s0 and S1–s2, respectively. The black, red and blue lines represent the time-domain signals for 0 (i.e., initial state), 10% and 30% increase of the third-order elastic constants, respectively. The amplitude of the second harmonic increases with increasing third-order elastic constants of the material. The change rate α of normalized A_2/A_1^2 with the third-order elastic constants is defined as the sensitivity. Figure 6 shows the change of normalized A_2/A_1^2 as a function of the third-order elastic constants for mode pairs S0–s0 and S1–s2 at the propagation distance of 100 mm. In comparison, α of the mode pair S1–s2 is noticeably larger than that of the mode pair S0–s0. When the third-order elastic constants
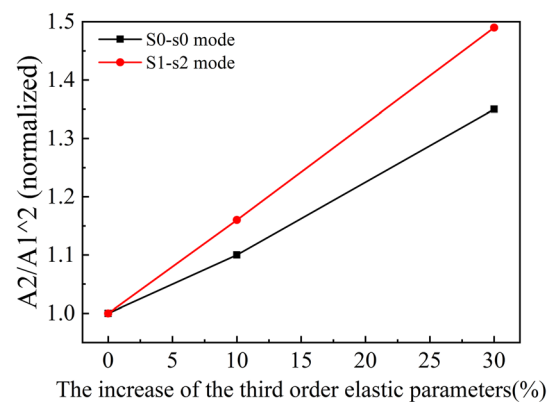

Fig. 6 Normalized relative acoustic nonlinearity parameter A_2/A_1^2 as a function of the third-order elastic constants for mode pairs S0–s0 and S1–s2 at the propagation distance of 100 mm
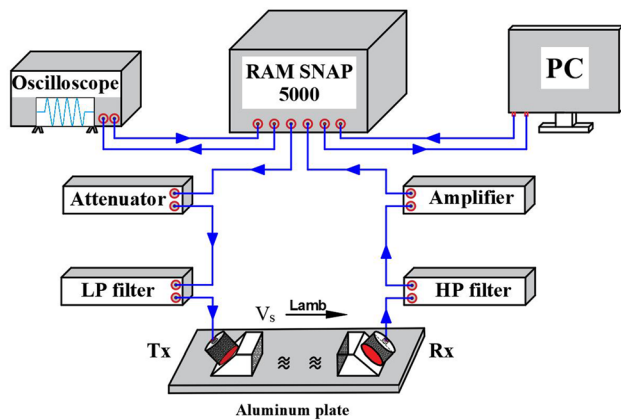
Fig. 7 Schematic of the experimental setup for the nonlinear ultrasonic Lamb waves measurements
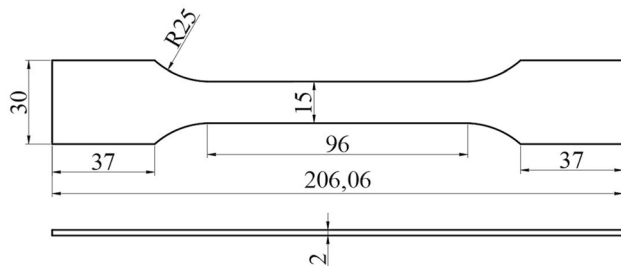

Fig. 8 Schematic diagram of the fatigue specimen. All dimensions are in mm

increase by 30%, α_{S1-s2} is 1.49 and α_{S0-s0} is 1.35. The mode pair S1–s2 is more sensitive to the change of the third-order elastic constants than S00.

4 Experiments

4.1 Experimental Setup and Specimen Preparation

A 7075 aluminum alloy was used in the experiments, whose material parameters were listed in Table 1. The longitudinal velocity, shear velocity, density and Poisson's ratio were 6372.7 m/s, 3146.2 m/s, 2.757 kg/m³, and 0.338, respectively. The experimental setup is schematically illustrated in Fig. 7. A high-power gated amplifier (RITEC SNAP RAM-5000, RITEC Inc., Warwick, RI, USA) and a wedge piezoelectric transducer were used to generate tone burst signal. In addition, it also consisted of a high-power attenuator, a pre-amplifier, low and high pass filters, an oscilloscope and a computer.

Figure 8 shows the nominal dimension of the flat dogbone specimen. The surface of each specimen was mechanically polished to a final roughness of ~ 0.2 μm. The two sides

of the specimen were clamped and the middle parallel section was used for the nonlinear ultrasonic Lamb waves measurements. Instron hydraulic servo universal testing system (8803 Floor Model Fatigue Testing system) was employed to conduct the low-cycle fatigue testing under laboratory environment. The specimens were subjected to the fatigue tests under the stress-control using a sinusoidal waveform with a constant frequency of 3 Hz and a stress ratio of 0.1. In the fatigue experiment, the average stress σ_m is 198 MPa, and the stress amplitude σ_a is 162 MPa.

Interruption fatigue test was conducted, namely, the specimen was loaded with a certain pre-determined number of cycles, and then unloaded (i.e., with 0 stress) to carry out the nonlinear ultrasonic Lamb waves measurement. When the nonlinear ultrasonic Lamb waves measurement was completed, the specimen was put back to the fatigue test machine and loaded again with the fatigue stress. The above process was repeated until the end of the predetermined cycles or fracture. One pristine specimen was employed to calibrate the measurement system before each nonlinear ultrasonic measurement on damaged specimens. In addition, a series of undamaged specimens with slight difference in the relative acoustic nonlinearity parameter A_2/A_1^2 were selected for the interruption fatigue tests.

4.2 Nonlinear Ultrasonic Lamb Waves Measurements

In the experimental measurements, the longitudinal piezoelectric transducers were coupled to the plexiglas wedges and specimens with light lubrication oil were used for the excitation and the reception of Lamb waves signals. In order to minimize measurement errors caused by uneven contact force artificially applied during the coupling process, a special fixture was uniformly used. The excitation frequency of Lamb waves mode pair S0–s0 was determined to be 300 kHz according to the FE simulations. A transducer with a center frequency of 300 kHz and a longitudinal piezoelectric transducer with a center frequency of 600 kHz were selected to excite and to receive propagation signals, respectively. An incident angle of 29.5° was set for Lamb waves mode pair S0–s0 according to Snell's law by $sin\theta = C_{wedge-l}\big/ C_p^{(\omega)}$. The frequency sweep analysis of Lamb waves mode pair S1–s2 was done before experimental measurements. The amplitude maximum of the second harmonic appeared at an excitation frequency of 2 MHz. Therefore, the excitation frequency of Lamb waves mode pair S1–s2 was set as 2 MHz in the experimental measurements. The S1 mode Lamb waves were excited by a longitudinal piezoelectric transducer with a central frequency of 2.25 MHz. Since the amplitude of the second harmonic is much smaller than that of the primary, a wide-band transducer with a central frequency of 5 MHz

was selected for receiving the nonlinear Lamb waves signals. All transducers used here are Olympus commercial probes. An incident angle θ of 24.5° satisfies Snell's law for Lamb waves mode pair S1–s2. The difference between the actual excitation frequency in the experimental measurements and the predicted one might be attributed to the calculation error of the dispersion curve, interference of other modes in the dispersion curve, the influence of the filter and other electronic components, and/or operational errors in the process of the experimental measurements.

The time-domain signals were analyzed by STFT to obtain the relative acoustic nonlinearity parameters A_2/A_1^2 at a propagation distance of 60 mm. The calibration was carried out by normalizing the A_2/A_1^2 to the initial value of 8.85×10^{-3} and 2.74 for mode pairs S0–s0 and S1–s2, respectively. Figure 9a and b show the normalized relative acoustic nonlinearity parameters A_2/A_1^2 as a function of the fatigue life for the specimen fractured at 24.5 thousand loading cycles. The normalized A_2/A_1^2F of both two mode pairs shows a mountain-shape dependence on the fatigue life fraction. The profile is similar for both mode pairs, but the value of normalized A_2/A_1^2 is quite different.

At the incipient stage, the normalized relative acoustic nonlinearity parameter A_2/A_1^2 increases substantially with the fatigue life. The normalized A_2/A_1^2 reaches its maximum at about 60% of the fatigue life, and then decreases with the fatigue cycles. The variation of the normalized A_2/A_1^2 of the mode pair S0–s0 is relatively small as compared with that of the mode pair S1–s2, with a change at the maximum of about 3.9% of its minimum value. However, the variation of the normalized A_2/A_1^2 of mode pair S1–s2 reaches about 42% of its minimum value. The variation of the normalized A_2/A_1^2 of mode pair S1–s2 is much larger than that of mode pair S0–s0. Consequently, the Lamb waves mode pair S1–s2 is more effective for evaluating the evolution of fatigue damages, which may be attributed to the quasi phase-velocity

matching of mode pair S0–s0, while the condition of strict phase-velocity matching is satisfied for mode pair S1–s2.

The slope of the relative acoustic nonlinearity parameter A_2/A_1^2 as a function of the propagation distance is defined as the excitation efficiency parameter γ [35]. Figure 10 shows the normalized A_2/A_1^2 of mode pairs S0–s0 and S1–s2 as a function of the propagation distance. The A_2/A_1^2 was normalized to the value at the propagation distance of 30 mm and 50 mm in FE simulations and experiments, respectively. It can be seen that the excitation efficiency parameter γ_{S1-s2} is much larger than γ_{S0-s0}. Simulation results show that the excitation efficiency of the mode pair S1–s2 is 2.13 times higher than that of the mode pair S0–s0. Experimental results show that the excitation efficiency of the mode pair S1- s2 is 4.85 times higher than that of the mode pair S0–s0. In FE simulations, the in-plane displacement signals were received and analyzed to calculate the excitation efficiency. The transducers with wedges were used in the experimental measurements to receive both the in-plane and the out-of-plane displacements. This may lead to the difference of the excitation efficiency between the experimental measurements and FE simulations. The results show that the mode pair S1–s2 has higher excitation efficiency and can better excite nonlinear ultrasonic Lamb waves, which is conducive to practical applications.

5 Results and discussion

The acoustic nonlinearity parameter presented in the previous experimental measurements show a mountain-shape curve versus the fatigue life. In addition, in view of the higher sensitivity of the mode pair S1–s2 to fatigue damage, it was used again to characterize the formation and propagation of fatigue-induced micro-cracks. Before the interruption fatigue test, one small hole was prefabricated in the middle
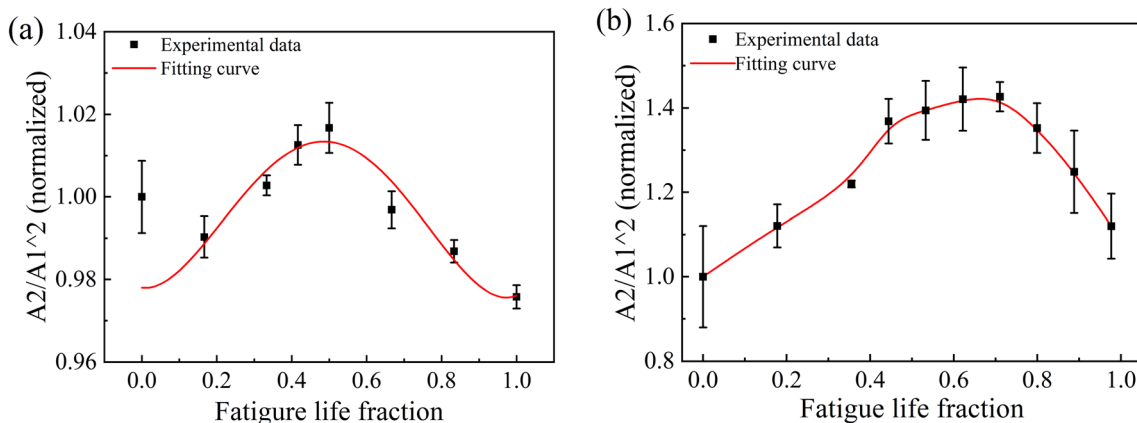

Fig. 9 Normalized relative acoustic nonlinearity parameter A_2/A_1^2 as a function of the fatigue life fraction: **b** mode pair S0–s0; **b**mode pair S1–s2
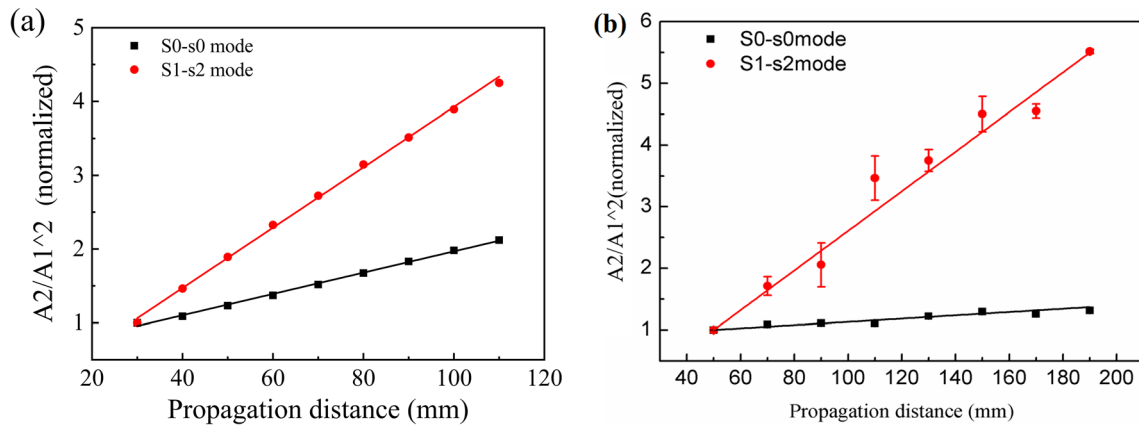
Fig. 10 Normalized relative acoustic nonlinearity parameter A_2/A_1^2 as a function of the propagation distance: **a** FE simulations; **b** Experiments
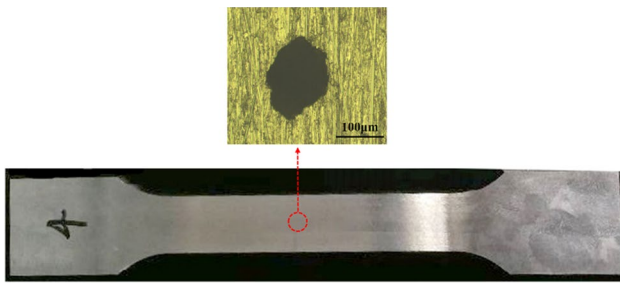

Fig. 11 The original specimen with a small hole

of each specimen as the source of crack initiation by laser ablation, as shown in Fig. 11. The interruption fatigue test was performed on three specimens. The small holes of these three specimens are shown in Fig. 12. The depth and diameter of the small hole were about 1 mm and 100 µm, respectively. The acoustic nonlinearity parameter was obtained at different fatigue cycles. For each specimen, nonlinear ultrasonic measurements were repeated five times at each propagation distance by completely removing and then reattaching the wedge transducer assembly to the plate. Meanwhile, the formation and growth of micro-cracks near the holes were observed by means of an optical microscope. In order to determine the stability of the measurement system and the

experimental process, the undamaged specimen was used as a reference during the experimental measurements. The normalized relative acoustic nonlinearity parameter as a function of the fatigue period was shown in Fig. 13, where the black and red points are the measured data of the normalized A_1 and the normalized A_2/A_1^2, respectively, while the black and red curves are the corresponding fitting curves. The relative acoustic nonlinearity parameter shows a mountain shape, reaching the maximum at around 60% fatigue life, and the corresponding number of fatigue cycles is about 150 k.
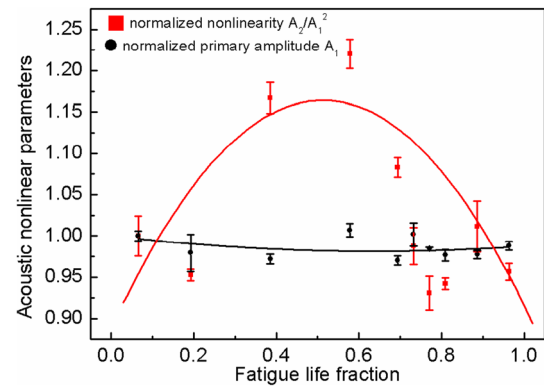

Fig. 13 Relative acoustic nonlinearity parameter A_2/A_1^2 as a function of the fatigue life fraction for mode pair S1–s2
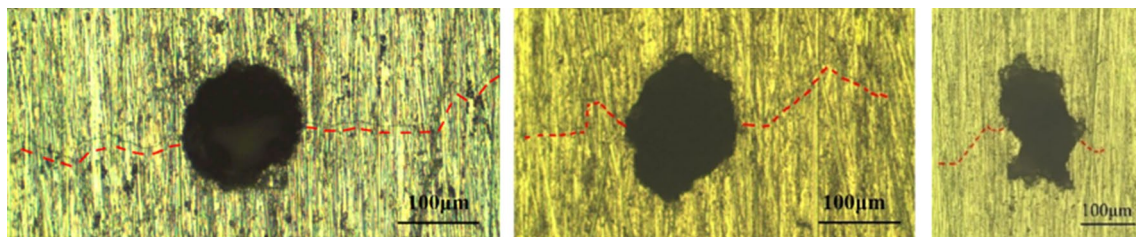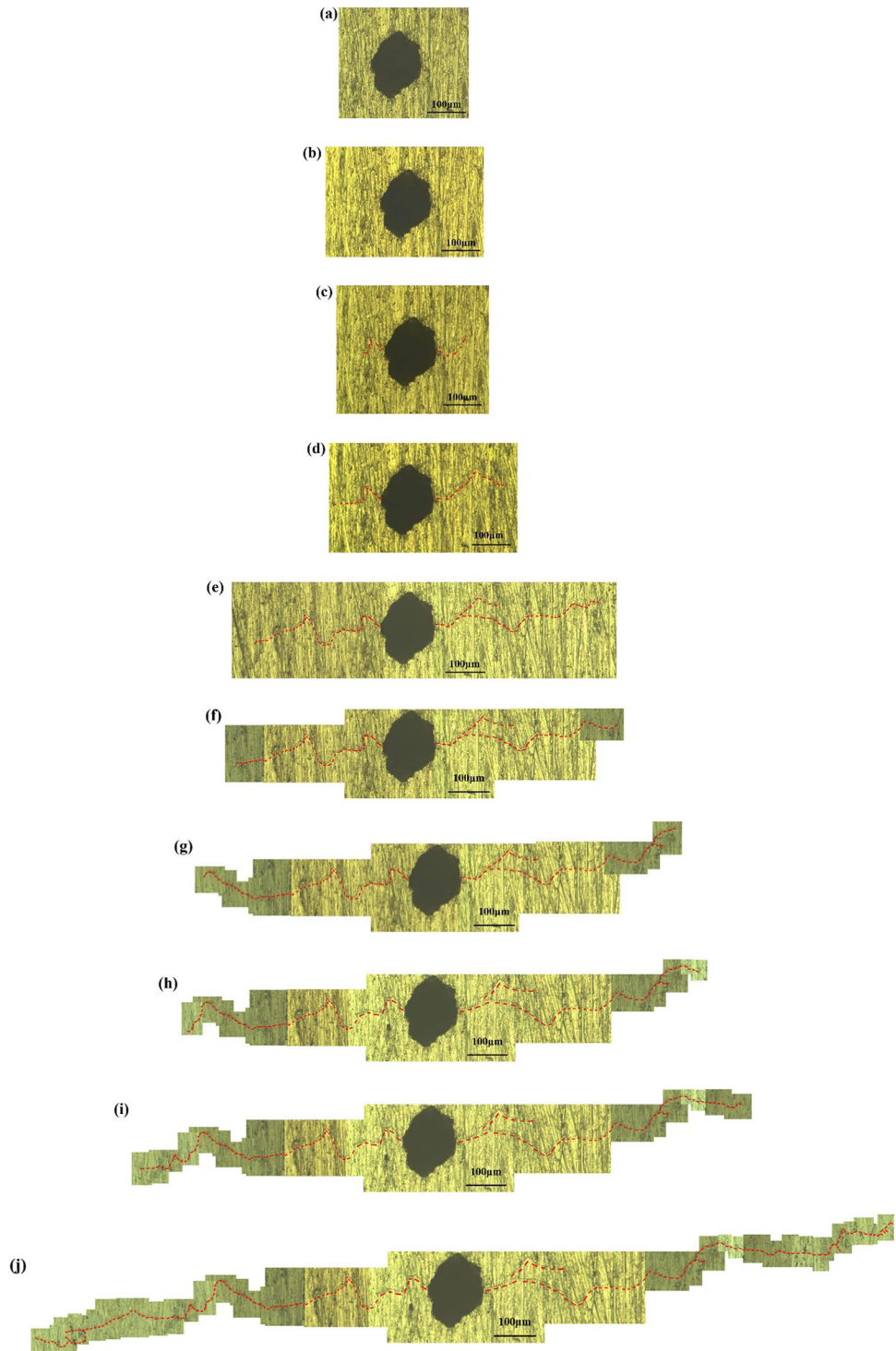

Fig. 12 Micrographs of small holes in three specimens

Fig. 14 Micrographs of microcracks at **a** 0, **b** 50, **c** 100, **d** 150, **e** 170, **f** 180, **g** 190, **h** 200, **i** 220 and **j** 240 thousand fatigue cycles

A Zeiss optical metallographic microscope (Observer. A1m, Zeiss, Germany) was used to observe the micro-crack. Figures 14 and 15 show the micrographs of the micro-crack at various loading cycles, where the red lines represent the micro-crack propagation paths. Only one main micro-crack initiates and propagates in each specimen. The micro-crack propagation can be found at two edges of the same hole. The micro-crack lengths and widths were quantitatively obtained based on these micrographs, as illustrated in Fig. 16. The acoustic nonlinearity acquired in our experimental

Fig. 15 The cracks width at **a** 220 thousand and **b** 240 thousand cycles
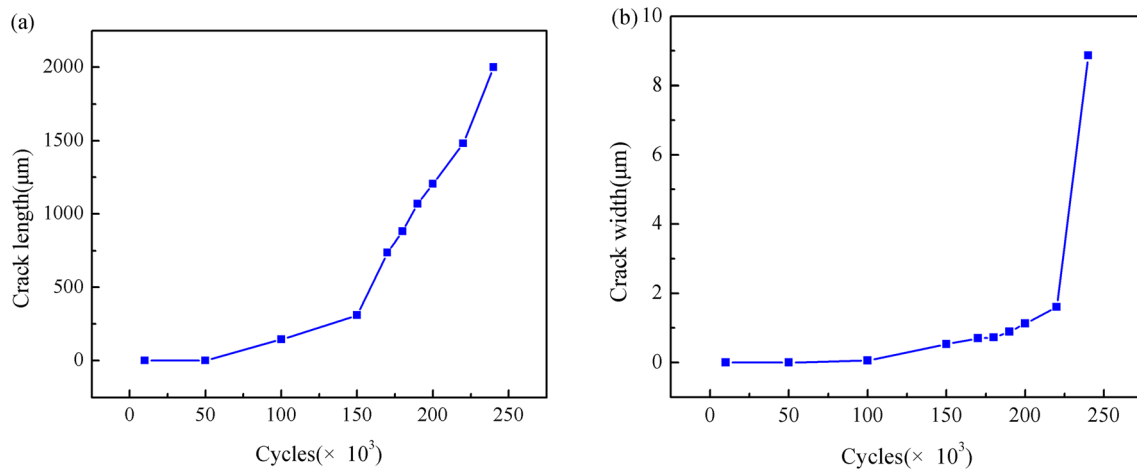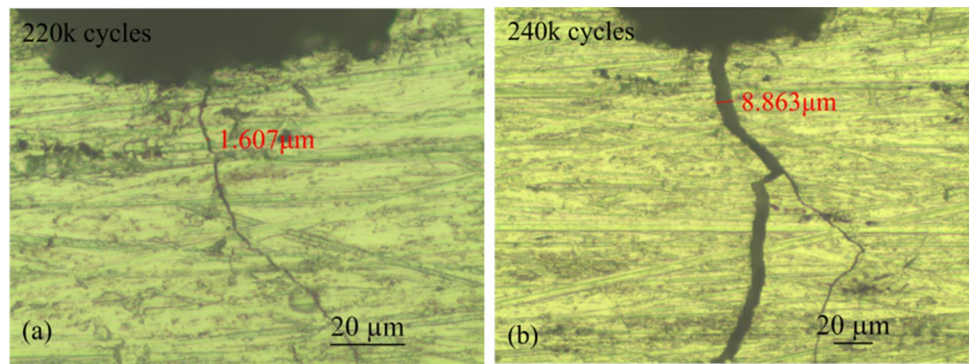

Fig. 16 **a** Crack length and **b** crack width versus the loading cycles

measurements is generated mainly from one crack in each specimen. It could be found that the micro-crack width barely changes before 150 thousand fatigue cycles, while the micro-crack length increases obviously. Therefore, the increase of the relative acoustic nonlinearity parameter is mainly attributed to the increase of the micro-crack length at the incipient stage. The increase of the micro-crack width may lead to a decrease of the relative acoustic nonlinearity parameter. In the later stage, as both the micro-crack length and width grow with the fatigue cycles, the contribution of the micro-crack width overcomes that of the micro-crack length to the relative acoustic nonlinearity parameter. As a result, the relative acoustic nonlinearity parameter starts to decrease.

The experimental results show that the length of the fatigue micro-cracks has a major effect on the relative acoustic nonlinearity parameter at the incipient stage of fatigue damage. The relative acoustic nonlinearity parameter increases with increasing length of the fatigue macro-cracks. In the later stage of fatigue damage, the width of the fatigue micro-cracks has a predominant effect on the relative acoustic nonlinearity parameter. The relative acoustic

nonlinearity parameter decreases with increasing width of the fatigue cracks. Our results can be used to explain relationship between the relative acoustic nonlinearity parameter and the evolution of fatigue-induced micro-cracks.

6 Conclusion

In this paper, experimental measurements and FE simulations were performed to study the ultrasonic nonlinear responses from the fatigue damage in 7075 aluminum alloy plates. A FE simulation model was presented to investigate the behavior of nonlinear ultrasonic Lamb waves propagation associated with the material and the fatigue damage. The FE simulations focus on possible contributions of the third-order elastic constants to the acoustic nonlinearity parameter. Results show that the sensitivity of the mode pair S1–s2 is 1.1 times higher than that of the mode pair S0–s0, when the third-order elastic constants increase by 10% and 30%, respectively. Meanwhile, the excitation efficiency of mode pairs S0–s0 and S1–s2 was quantitatively analyzed. Results from the simulation and the experiments show that

the excitation efficiency of the mode pair S1–s2 is much higher than that of S0–s0.

In addition, the normalized A_2/A_1^2 of the two mode pairs shows a mountain-shape curve as a function of the fatigue cycles, and the maximum appears at about 60% of the fatigue life. The normalized A_2/A_1^2 changes by about 3.9% and 42% of its respective initial values for the mode pairs S0–s0 and S1–s2, respectively. Therefore, the mode pair S1–s2 is more sensitive to evaluate the fatigue damage. The relationship between the length and width of the fatigue-induced microcracks and the relative acoustic nonlinearity parameter is established. Below a length of about 300 μm, the microcrack width changes little, and the relative acoustic nonlinearity parameter increases with the micro-crack length. When the length is larger than 300 μm, the micro-crack width increases rapidly, and the relative acoustic nonlinearity parameter decreases with increasing micro-crack width. Thus, it confirms the effect of fatigue damage on generation of nonlinear ultrasonic Lamb waves.

References

1. Meyendorf, N.G., Rosner, H., Kramb, V., et al.: Thermo-acoustic fatigue characterization. Ultrasonics **40**(1–8), 427–434 (2002)
2. Cantrell, J.H.: Substructural organization, dislocation plasticity and harmonic generation in cyclically stressed wavy slip metals. Proc. Math. Phys. Eng. Sci. **460**(2043), 757–780 (2004)
3. Sagar, S.P., Das, S., Parida, N., et al.: Non-linear ultrasonic technique to assess fatigue damage in structural steel. Scr. Mater. **55**(2), 199–202 (2006)
4. Baby, S., Kowmudi, B.N., Omprakash, C.M., et al.: Creep damage assessment in titanium alloy using a nonlinear ultrasonic technique. Scr. Mater. **59**(8), 818–821 (2008)
5. Cantrell, J.H., Salama, K.: Acoustoelastic characterisation of materials. Int. Mater. Rev. **36**(1), 125–145 (1991)
6. Jhang, K.Y., Kim, K.C.: Evaluation of material degradation using nonlinear acoustic effect. Ultrasonics **37**(1), 39–44 (1999)
7. Deng, M.X., Xiang, Y.X., Liu, L.B.: Time-domain analysis and experimental examination of cumulative second-harmonic generation by primary lamb wave propagation. J. Appl. Phys. **109**(11), 1829–1836 (2011)
8. Liu, M.G., Kim, J.Y., Jacobs, L., et al.: Experimental study of nonlinear rayleigh wave propagation in shot-peened aluminum plates-feasibility of measuring residual stress. NDT and E Int. **44**(1), 67–74 (2011)
9. Doerr, C., Lakocy, A., Kim, J.Y., et al.: Evaluation of the heat-affected zone (haz) of a weld joint using nonlinear rayleigh waves. Mater. Lett. **190**, 221–224 (2017)
10. Shen, Y., Cesnik, C.E.: Modeling of nonlinear interactions between guided waves and fatigue cracks using local interaction simulation approach. Ultrasonics. **74**, 106123 (2017)
11. Wang, Y., Guan, R., Lu, Y.: Nonlinear lamb waves for fatigue damage identification in frp-reinforced steel plates. Ultrasonics **80**, 87–95 (2017)
12. Yang, Y., Ng, C.T., Kotousov, A., et al.: Second harmonic generation at fatigue cracks by low-frequency Lamb waves: experimental and numerical studies. Mech. Syst. Signal Process. **99**, 760–773 (2018)
13. Jhang, K.Y.: Nonlinear ultrasonic techniques for nondestructive assessment of micro damage in material: a review. Int. J. Precis. Eng. Manuf. **10**(1), 123–135 (2009)
14. Chillara, V.K., Lissenden, C.J.: Review of nonlinear ultrasonic guided wave nondestructive evaluation: theory, numerics, and experiments. Opt. Eng. **55**(1), 011002.1–011002.15 (2016)
15. Broda, D., Staszewski, W.J., Martowicz, A., et al.: Modelling of nonlinear crack–wave interactions for damage detection based on ultrasound-a review. J. Sound Vib. **333**(4), 1097–1118 (2014)
16. Zhu, W.J., Xiang, Y.X., Liu, C.J., et al.: Fatigue damage evaluation using nonlinear lamb waves with quasi phase-velocity matching at low frequency. Materials. **11**(10), 1920 (2018)
17. Metya, A.K., Ghosh, M., Parida, N., et al.: Effect of tempering temperatures on nonlinear lamb wave signal of modified 9cr-1Mo steel. Mater. Charact. **107**, 14–22 (2015)
18. Xiang, Y.X., Deng, M.X., Xuan, F.Z.: Creep damage characterization using nonlinear ultrasonic guided wave method: a mesoscale model. J. Appl. Phys. **115**(4), 273 (2014)
19. Jhang, K.Y.: Applications of Nonlinear Ultrasonics to the NDE of Material Degradation. IEEE Trans. Ultrason. Ferroelectr. Freq. Control **47**(3), 540–548 (2000)
20. Kim, C.S., Kim, Y.H., Kim, I.H.: Ultrasonic linear and nonlinear parameters in cyclically deformed Cu and Cu-35Zn alloy. Key Eng. Mater. **297–300**(Pt3), 2134–2139 (2005)
21. Deng, M.X., Pei, J.F.: Assessment of accumulated fatigue damage in solid plates using nonlinear Lamb wave approach. Appl. Phys. Lett. **90**(12), 273–277 (2007)
22. Sagar, S.P., Metya, A.K., Ghosh, M., et al.: Effect of microstructure on non-linear behavior of ultrasound during low cycle fatigue of pearlitic steels. Mater. ence Eng. A **528**(6), 2895–2898 (2011)
23. Steven, V.B., Kong, C.W., Francis, R.L.: Experimental investigation of second-harmonic lamb wave generation in additively manufactured aluminum. J. Nondestr. Eval. Diagn. Progn. Eng. Syst. **1**(4), 041003 (2018)
24. Pruell, C., Kim, J.Y., Qu, J., et al.: Evaluation of fatigue damage using nonlinear guided waves. Smart Mater. Struct. **18**(3), 035003 (2009)
25. Jin, H.S., Yan, J.J., Li, W.B., et al.: Monitoring of fatigue crack propagation by damage index of ultrasonic guided waves calculated by various acoustic features. Appl. Sci. **9**(20), 4254 (2019)
26. Jingpin, J., Xiangji, M., Cunfu, H., Bin, W.: Nonlinear lamb wave-mixing technique for micro-crack detection in plates. Ndt & E Int. **85**, 63–71 (2017)
27. Wan, X., Zhang, Q., Xu, G., et al.: Numerical simulation of nonlinear lamb waves used in a thin plate for detecting buried microcracks. Sensors **15**(5), 8528–8546 (2014)
28. Shen, Y.F., Wang, J.Z., Xu, W.: Nonlinear features of guided wave scattering from rivet hole nucleated fatigue cracks considering the rough contact surface condition. Smart Mater. Struct. **27**(10), 105044 (2018)
29. Wang, J.W., Shen, Y.F., Rao, D.Y., et al.: An instantaneous-baseline multi-indicial nonlinear ultrasonic resonance spectral correlation technique for fatigue crack detection and quantification. Nonlinear Dyn. (2021). https://doi.org/10.1007/s11071-020-06128-x

30. Liu, P.P., Jang, J.H., Yang, S.Y., et al.: Fatigue crack detection using dual laser induced nonlinear ultrasonic modulation. Opt. Lasers Eng. **110**, 420–430 (2018)
31. Viktorov, I.A.: Rayleigh and Lamb Waves: Physical Theory and Applications. Plenum Press, New York (1967)
32. Li, W.B., Cho, Y.H., Achenbach, J.D.: Detection of thermal fatigue in composites by second harmonic Lamb waves. Smart Mater. Struct. **21**(8), 85019–85026 (2012)
33. Sun, M.X., Xiang, Y.X., Deng, M.X., et al.: Scanning non-collinear wave mixing for nonlinear ultrasonic detection and localization of plasticity. NDT E Int. **93**, 1–6 (2018)
34. Zhu, W.J., Xiang, Y.X., Liu, C.J., et al.: A feasibility study on fatigue damage evaluation using nonlinear Lamb waves with group-velocity mismatching. Ultrasonics **90**, 18–22 (2018)
35. Matlack, K.H., Kim, J.Y., Jacobs, L.J., et al.: Experimental characterization of efficient second harmonic generation of lamb wave modes in a nonlinear elastic isotropic plate. J. Appl. Phys. **109**(1), 2141 (2011)